ACS OMEGA

http://pubs.acs.org/journal/acsodf

Article

Applications of Mesoporous Silica-Encapsulated Gold Nanorods Loaded Doxorubicin in Chemo-photothermal Therapy

Nghiem Thi Ha Lien,* Anh D. Phan,* Bui Thi Van Khanh, Nguyen Thi Thuy, Nguyen Trong Nghia, Hoang Thi My Nhung, Tran Hong Nhung, Do Quang Hoa, Vu Duong, and Nguyen Minh Hue

Cite This: *ACS Omega* 2020, 5, 20231−20237

Read Online

ACCESS | Metrics & More | Article Recommendations | Supporting Information

ABSTRACT: We investigate the chemo-photothermal effects of gold nanorods (GNRs) coated using mesoporous silica ($mSiO_2$) loading doxorubicin (DOX). When the mesoporous silica layer is embedded by doxorubicin drugs, a significant change in absorption spectra enables to quantify the drug loading. We carried out photothermal experiments on saline and livers of mice having GNRs@$mSiO_2$ and GNRs@$mSiO_2$-DOX. We also injected the gold nanostructures into many tumor-implanted mice and used laser illumination on some of them. By measuring the weight and size of tumors, the distinct efficiency of photothermal therapy and chemotherapy on treatment is determined. We experimentally confirm the accumulation of gold nanostructures in the liver.

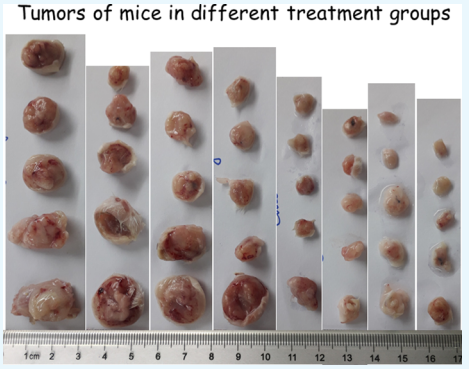

INTRODUCTION

Photothermal effects of gold nanorods have been extensively investigated due to medical applications.[1−6] When illuminated by light, gold nanorods (GNRs) absorb radiation and confine electromagnetic energy to the surface of a gold−dielectric interface. The absorbed energy is efficiently transformed into thermal energy and locally heats to a few hundred degrees Celsius under the illumination of laser light. Since the destruction of living cells occurs at temperatures above 43 °C, this light-to-heat conversion process is used for cancer therapy.[1−6] In the synthesis of gold nanostructures using cetyl trimethylammonium bromide (CTAB), their gold surfaces become unstable and easily aggregate. This aggregation causes the loss of unique optical properties. Moreover, it has been proved that CTAB is a highly toxic cationic surfactant.[7,8] To exploit GNRs for biomedical applications, it is necessary to replace CTAB and coat GNRs by safer and more biocompatible materials/molecules. Recently, extensive efforts have been devoted to encapsulate GNRs with mesoporous silica,[9,10] biopolymers,[11,12] or other composites.[13,14] These coating materials can be easily combined with drugs or target molecules to functionalize GNRs.

In some biological and photothermal applications, GNRs is preferred rather than gold nanoshells (GNSs) because of two main reasons. First, the size of GNSs having plasmon resonances in the near-infrared region is large (∼150 nm),[15,16] while the size of GNRs is small (≤80 nm).[1−6] According to previous works,[17,18] sub-100 nm nanoparticles are selected for treatments due to their free movement through tissues. Second, it is well known that GNRs have a strong optical absorption cross section and a very small scattering cross section.[19,20] These behaviors are relatively opposite to properties of large-size GNSs. Thus, the GNRs are more photothermally efficient than the GNSs.[19,20]

While doxorubicin (DOX) is an anthracycline antibiotic known as one of the most therapeutic antitumor drugs to treat various solid malignant tumors. Doxorubicin intercalates within DNA helix in the cell nucleus. Thereby, this drug inhibits macromolecular biosynthesis and destroys the DNA function.[21] However, free doxorubicin has its own several side effects when used in cancer chemotherapy.[22] To reduce the toxicity and side effects and improve treatment efficiency, one encapsulates DOX in liposomes,[23] loads onto silica mesoporous nanoparticles,[24] or incorporates into nanocomposites such as silica mesoporous encapsulated GNRs,[25] GNR@$mSiO_2$, or GNR@polymers.[9,12] Doxorubicin release and loading from GNR@$mSiO_2$-DOX or GNR@polymer-DOX strongly depend on the acidic medium and laser irradiation at surface plasmon resonances.[9] The synergistic effect of the drug-loaded GNR@SiO_2 has been demonstrated.[9,14,22]

Recently, clinical trials have been performed for gold-nanoparticle-based photothermal cancer therapy to ablate thermally neck, brain, lung, and prostate cancerous tu-

Received: April 27, 2020
Accepted: July 24, 2020
Published: August 7, 2020

https://dx.doi.org/10.1021/acsomega.0c01939
ACS Omega 2020, 5, 20231−20237

mors.[9,26−28] These results showed promising scenarios since tumors were locally heated. However, the accumulation of gold nanostructures in the liver and spleen throughout life in bodies without excretion is the weakest point of this approach.[27,28] The penetration of gold composites into tumors is tiny compared to the infused initial counterparts.

In this work, we synthesize GNRs@mSiO$_2$-DOX and investigate photothermal and chemical behaviors of nanostructures under laser irradiation. We use transmission electron microscopy (TEM) and X-ray diffraction (XRD) spectrum to analyze the structures of experimental samples. The effects of DOX loading on optical properties are determined using the absorption spectrum. Then, we inject solutions of GNRs@mSiO$_2$ with and without DOX molecules into 45 normal and tumor-planted mice and study the chemo-photothermal activities. Based on experimental results, we quantitatively evaluate the roles of individual mechanisms on cancer treatments.

EXPERIMENTAL SECTION

Materials. We purchased tetrachloroauric acid trihydrate 99.5% (HAuCl$_4$·3H$_2$O), ethanol, CTAB, ascorbic acid, and AgNO$_3$ from Merck. Tetraethoxylsilane, NH$_4$OH (28−30%), and NaBH$_4$ were purchased from Sigma-Aldrich and Walko, respectively. Doxorubicin hydrochloride 2 mg/mL was provided by Ebewe Pharma. In our experiments, we dispersed materials into double distilled water.

Preparation and Characterization of GNR@SiO$_2$-DOX Complex. The synthesis of GNR@SiO$_2$-DOX composites consists of three steps. First, we synthesized near-infrared light-responsive GNRs. Second, a mesoporous silica layer is coated on gold surfaces. The thickness of the silica layer is approximately 15 nm. Third, when dispersing DOX·HCl molecules in an aqueous solution of GNSs, the mesoporous silica surface adsorbed the biomolecules onto the mesoporous silica surface via electrostatic interactions. Finally, we obtained mesoporous silica-encapsulated GNR (GNR@mSiO$_2$-DOX) composites loading DOX molecules.

Preparation of GNRs. Gold nanorods having dimensions of ∼39.2 × 10.7 nm^2 (an average aspect ratio of 3.7) were synthesized using the seed-mediated growth method.[29] Briefly, the seed was made by stirring 120 μL of 25 mM HAuCl$_4$ in 10 mL of 100 mM CTAB solution. Then, we quickly added ice-cold NaBH$_4$ (60 μL, 10 mM) to the seed solution and stirred for 2−6 h. By mixing 100 mL of CTAB 100 mM, 1.5 mL of HAuCl$_4$ 25 mM, 450 μL of AgNO$_3$ 25 mM, and 270 μL of L-ascorbic acid 100 mM, a growth solution was prepared. After 2 h of reaction in a mixture of 1000 μL of the seed solution and the growth solution, the GNR seeds were synthesized.

Preparation of Mesoporous Silica-Encapsulated GNRs. GNRs were prepared by a seed-mediated sequential growth and a reduction of gold salt in the presence of a CTAB surfactant. A 20 mL aliquot of the GNR solution was centrifuged and redispersed in 20 mL of deionized water. Then, we added 0.5 mL of the TEOS ethanol solution (20 mM) to 20 mL of the GNR aqueous solution (pH is adjusted to 10−11 by mixing NH$_4$OH). After vigorously stirring for 24 h at room temperature, a 15 nm thick mesoporous silica layer was formed on the surface of the GNRs through hydrolysis and condensation of TEOS. The silica-encapsulated GNRs were isolated by centrifugation, washed with deionized water and ethanol several times, and then redispersed in 2 mL of deionized water for later use.

Mesoporous Silica-Encapsulated GNRs Functionalized with Doxorubicin Drugs. We added 200 μL of DOX·HCl 2 mg/mL solution to a solution of GNRs@mSiO$_2$ solution, which has the optical density (OD) equal to 12. Then, this mixture was stirred and mixed during 75 h at room temperature in the dark. Electrostatic interaction between doxorubicin molecules and the mesoporous silica surface leads to molecular adsorption at particle surfaces.[30,31] Finally, we used UV−vis−NIR spectrometer to monitor the adsorbing procedure of DOX into the mesoporous silica surface.

Measurements. In the final GNR suspension, GNRs@mSiO$_2$ and GNRs@SiO$_2$-DOX were characterized by an ultraviolet/visible wavelength (UV−vis−NIR) spectrophotometer (Shimadzu 2600). We examined the sizes and shapes of GNRs by high-resolution transmission electron microscopy (HRTEM, JEM2100-JEOL). The samples were prepared by placing one drop of the GNR suspension on a 200-mesh, copper grid with carbon (SPI Supplies, West Chester, Pennsylvania), and drying in a vacuum oven overnight. We used X-ray diffraction to determine the chemical composition and crystallinity of the obtained GNRs.

In Vivo Experiments. For in vivo experiments, we used healthy male Swiss Albino mice (8−10 weeks old) with a weight of 18 ± 1.5 g. The mice had free access to food and water and maintained on a 14/10 h light/dark cycle. The sarcoma cancer cells were subcutaneously implanted (2 × 10^6 cells/100 μL of Hank's solution) into the right side of the mouse back. The tumor size was measured daily. These animals were examined when their average tumor size grew up to 5−6 mm in diameter. We randomly divided 45 mice into nine groups (five mice per group): one control group and eight experimental groups with two different concentrations of GNR@mSiO$_2$ and GNR@mSiO$_2$-DOX having optical densities of 5.5 and 9.2 at 808 nm under 808 nm laser irradiation, respectively. Particularly, the groups are

Control group: without tumor and no treatment.
Group 1: saline injection.
Group 2: saline injection + 808 nm laser irradiation;
Group 3: GNR@mSiO$_2$ OD = 9.2.
Group 4: GNR@mSiO$_2$-DOX OD = 9.2
Group 5: GNR@mSiO$_2$ OD = 5.5 + 808 nm laser irradiation.
Group 6: GNR@mSiO$_2$ OD = 9.2 + 808 nm laser irradiation.
Group 7: GNR@mSiO$_2$-DOX OD = 5.5 + 808 nm laser irradiation.
Group 8: GNR@mSiO$_2$-DOX OD = 9.2 + 808 nm laser irradiation.

We used a 1 mL syringe with a 26G needle to inject directly 30 μL of phosphate-buffered saline (PBS) 1× or GNR@mSiO$_2$/GNR@SiO$_2$-DOX solutions into each tumor center of the mice. The animals were irradiated with laser (808 nm, 3.25 W/cm^2, 1 min, a spot size of 6 mm) immediately after direct tumor injection. The laser was focused at the center of the tumor. We measured the temperature rise of the tumor surface by an infrared (IR) camera (Chauvin Arnoux C.A 1995 IR camera IP 54). After treatment, we observed the health and weight of the mice. After 1 month, all mice were euthanized. We dissected their tumors and measured their weight. The average body weights of nine groups of mice as a function of time are shown in Figure S1 in the Supporting Information. At that time, we also analyzed blood chemistry and hematology.

https://dx.doi.org/10.1021/acsomega.0c01939
ACS Omega 2020, 5, 20231−20237

All experiments were performed in compliance with the policy on animal use and ethics.

RESULTS AND DISCUSSION

Figure 1a,1b shows the TEM images of a solution of GNRs and GNR@mSiO$_2$, respectively. The TEM images indicate

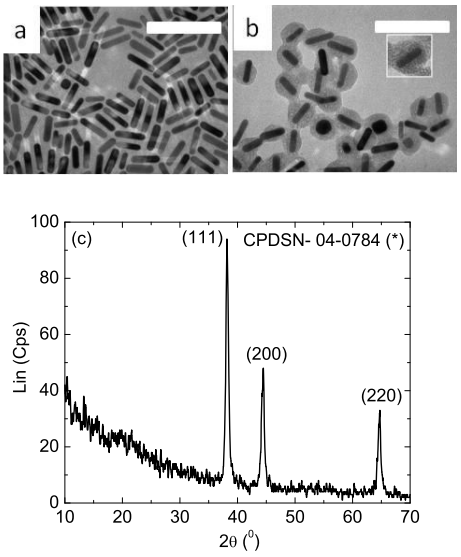

Figure 1. TEM image of (a) GNRs and (b) GNRs@mSiO2 with a scale bar of 100 nm. (c) X-ray diffraction spectrum of GNRs.

that the average length and width are 39.2 ± 6.2 and 10.7±1.7 nm, respectively (the average aspect ratio of 3.7). The silica shell is uniform and has a thickness of ∼15 nm. One can see a TEM image of the mesoporous silica coating on GNRs in Figure S2 in the Supporting Information.

Figure 1c shows X-ray diffraction of GNRs to determine their chemical composition and crystallinity. We find three characteristic diffraction peaks at 38.27, 44.42, and 64.70° corresponding to the (111), (200), and (220) crystal planes of the face-centered cubic structure of gold (JCPDS no. 04-0784), respectively. The presence of these optical maxima indicates a polycrystalline structure of GNRs. In addition, since there are no other impurities in the diffraction patterns, our samples are composed of pure crystalline gold.

Figure 2 shows the normalized absorption spectra of GNRs (or CTAB-GNRs) and GNR@mSiO$_2$. Note that GNRs have CTAB molecules on the surface to stabilize and avoid aggregation. In each spectrum, two peaks correspond to the

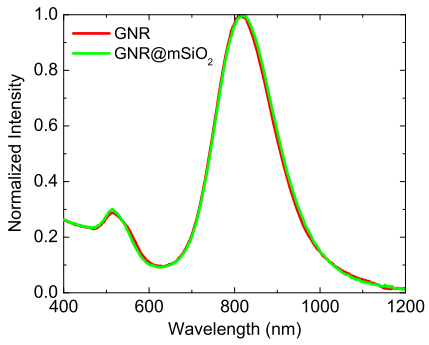

Figure 2. Normalized absorption spectra of GNRs and GNR@mSiO$_2$.

transverse (∼513 nm) and longitudinal (∼820 nm) oscillation. The surface plasmon resonance of GNRs is strongly dependent on their aspect ratio.[20] An increase in the aspect ratio leads to a red shift of the optical peak. However, our results indicate that the silica layer has a minor effect on the absorption spectrum. This may be due to a broad distribution of the rod length and width of GNRs as shown in Figure S3 in the Supporting Information. This behavior is completely consistent with the experimental results in ref 32.

Compared to the optical spectrum of CTAB-GNRs, the longitudinal surface plasmon resonance band of GNR@mSiO$_2$ is slightly red-shifted to about 6 nm. Meanwhile, the peak location for the transverse plasmon band of CTAB-GNRs is at 513 nm, and this resonance is blue-shifted about 4 nm when silica is coated on the gold surface. This behavior can be explained by the fact that the refractive index of silica shell (1.45) is closer to that of water media (1.33) than that of the 2−3 nm CTAB layer (1.49). It means the silica layer provides more transmission and lower reflection of electromagnetic fields than the CTAB layer. Thus, more electrons of the GNR core are excited to collectively resonate. The shift in optical resonances increasing the refractive index of the medium surrounding the core is predictable.

The DOX loading of GNRs@mSiO$_2$ can be analyzed using the absorption spectra. As shown in Figure 3, the absorption

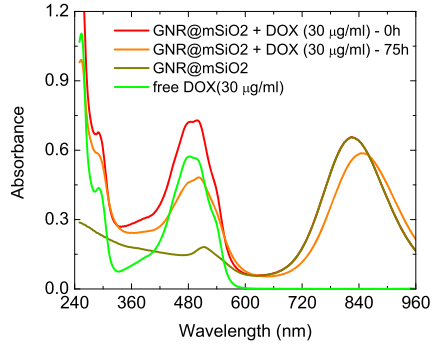

Figure 3. Absorption spectra of free DOX at a concentration of 30 μg/mL. GNR@mSiO$_2$ and GNR@mSiO$_2$-DOX (30 μg/mL) at 0 h and after 75 h of incubation.

spectra of GNR@mSiO$_2$ is blue-shifted after adsorbing DOX. Doxorubicin molecules in the mesoporous silica layer enhance the absorbance intensity of the transverse peak near 500 nm but do not affect the absorbance of the longitudinal peak located at about 813 nm. This is because DOX molecules strongly absorb light at 500 nm and do not interact with NIR radiation. After 75 h incubation, the optical spectrum of GNR@mSiO$_2$-DOX is lowered in comparison with the spectrum measured immediately before and after mixing with DOX. These results indicate that DOX molecules tightly bind to the silica layer of GNR@mSiO$_2$ but biological degradation may appear.[33]

Free and absorbed DOX molecules can be separated using centrifugation. We removed the supernatant with a pipette and determined the concentration of the residual DOX in the supernatant by measuring its absorbance and then comparing this measured spectrum with that of the known concentrations of free DOX solution. From this, we estimated that 1 μg of Au approximately absorbs 1.3 μg of DOX.

Under NIR 808 nm laser irradiation with power density at 3.25 W/cm^2 for 1 min, GNRs@mSiO$_2$ and GNRs@mSiO$_2$-

https://dx.doi.org/10.1021/acsomega.0c01939
ACS Omega 2020, 5, 20231−20237

DOX in solutions absorb light energy and convert it into heat. Solutions of plasmonic nanocomposites are fixed at the same optical density of 3.6 at 808 nm. During the laser illumination, as shown in Figure 4, the temperature of GNR@mSiO$_2$ and GNR@mSiO$_2$-DOX solutions rapidly increases from room temperature to approximately 70.5 °C. Theoretically, using the energy balance equation in homogeneous and open systems, one derives an analytical fitting function $T(t) = T_0 + (A/B)(1 - e^{-Bt})$ to describe the time-dependent temperature.[15,34] The analysis agrees quantitatively well with our experimental data. The temperature increases in these solutions relatively overlap. This result can be deduced from Figure 3 since the presence of DOX molecules does not alter the absorbance of GNR@mSiO$_2$ in the NIR region. Thus, aqueous solutions of GNR@mSiO$_2$ and GNR@mSiO$_2$-DOX absorb energy and are heated in the same manner. While the temperature is nearly unchanged in a saline solution.

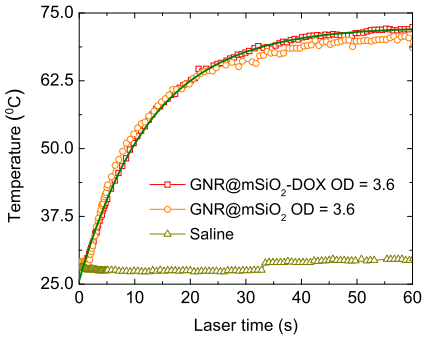

Figure 4. Time-dependent temperature of GNR@mSiO$_2$ and GNR@mSiO$_2$-DOX solutions with the optical density of 3.6 and saline irradiated with the NIR laser (808 nm, 3.25 W/cm^2). The solid curve is an analytic function $T(t) = T_0 + (A/B)(1 - e^{-Bt})$ with T_0 = 24.67 °C, $A \approx 3.168$ °C s, and $B = 0.0773$ s^{-1}.

Furthermore, since the absorption spectrum of GNRs with and without a mesoporous silica layer on the gold surface has a very small variation (see Figure 2), one could expect a perfect overlapping between the time-dependent temperature rise of GNR solution and that of the GNR@mSiO$_2$ solution.

Examining the chemo-photothermal effects of nanocomposites on animals is an essential part of a step toward practical applications. In addition to investigations of the time-dependent rise, the accumulation of nanostructures in the liver has been intensively studied in medicine-related fields. Several recent works used the dose for intravenous administration of GNRs ranging from 1.7 to 25 mg/kg.[9,35] It was proved that the amount of GNRs is accumulated in internal organs, particularly the liver and spleen, after infusion. In the remaining life, GNRs cannot be excreted from their bodies.[27] Another study showed that gold nanoparticles are mainly trapped in the Kuffer macrophage cells in the liver for 2 h after intravenous injection.[36]

In our work, to test the accumulation of GNR@mSiO$_2$ in the liver, we injected low doses (100 μL of saline buffer and GNR@mSiO$_2$ 1.75 mg/kg) into the mice. Two hours after intravenous injection, the mice were sacrificed and their livers were taken. The presence and influences of GNRs in the livers were determined via photothermal effects. Under the same conditions of in vivo experiments, we illuminated livers at the three different positions (P_1, P_2, and P_3 as depicted in Figure 5b,5d) within 2 min of NIR laser irradiation (808 nm, 3.25 W/cm^2). In livers without GNRs, Figure 5a,5b shows no difference (visual) between before and after laser radiation at three irradiated positions. Meanwhile, for livers of mice with tail vein injection of GNR@mSiO$_2$ solutions, one visually observes a color change of the liver after laser radiation in Figure 5d. The color at these three positions irradiated by laser turns yellow, as compared to that in Figure 5c. This indicates the presence of gold nanostructures in the liver, and the accumulation leads to the heat-induced denaturation of organs. The time-dependent temperature rises in livers at positions P_1, P_2, and P_3 in Figure 5b,d, which corresponds to samples injected with saline buffer and GNR@mSiO$_2$, respectively, were monitored and are shown in Figure 5e. The temperatures of the experimental samples with GNRs@mSiO$_2$ increase up to 85 ± 2 °C after 2 min. In the liver with only saline, the temperature slowly increases and reaches 44 ± 1 °C. There is not much difference between temperatures at the irradiated points. This finding suggests that the liver is an approximately homogeneous medium and GNRs@mSiO$_2$ are randomly distributed. Again, the mathematical form of the time-dependent temperature obeys the fit equation $T(t) = T_0 + (A/B)(1 - e^{-Bt})$.

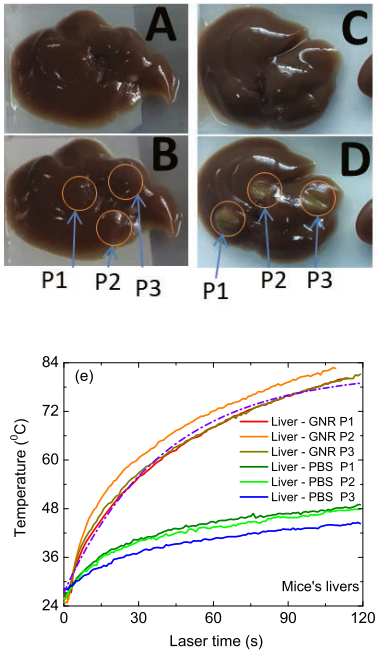

Figure 5. Images of the liver of control mice without GNR infusion before (a) and after (b) irradiation with NIR laser (808 nm, 3.25 W/cm^2, 2 min). Images of the liver of mice with 150 μL, OD = 10 of GNR@mSiO$_2$ infusion before (c) and after (c) NIR laser radiation (808 nm, 3.25 W/cm^2, 2 min). (e) Temperature rises in the liver of mice at the three different positions 2 h after vein tail injection in (b) and (d). The dashed-dotted violet curve is the analytic function $T(t) = T_0 + (A/B)(1 - e^{-Bt})$, where T_0 = 27.29 °C, $A \approx 1.36$ °C s, and $B = 0.025$ s^{-1}.

The chemo- and photothermal therapies in the mice due to the use of GNR@SiO$_2$ and GNR@SiO$_2$-DOX are also investigated by the implanted mouse tumor models, as described in In Vivo Experiments Section. Figure 6a shows the photographs of tumors taken from eight animal groups 30 days after treatment. We measured the average tumor weight of each group. The results are shown in Figure 6b to quantify the contribution of chemotherapy and photothermal therapy. Overall, the presence of GNR@SiO$_2$ and GNR@SiO$_2$-DOX

https://dx.doi.org/10.1021/acsomega.0c01939
ACS Omega 2020, 5, 20231−20237

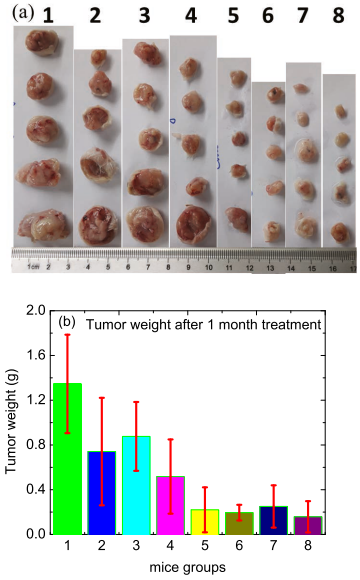

Figure 6. (a) Photograph of tumors after excision from eight groups: (1) untreated group; (2) laser only; (3) treatment with GNR@SiO_2 OD = 9.2; (4) treatment with GNR@SiO_2-DOX OD = 9.2; (5) and (6) treatment with GNR@SiO_2 OD = 5.5 and 9.2, respectively; (7) and (8) treatment with GNR@SiO_2-DOX OD = 5.5 and 9.2, respectively; and under NIR laser irradiation (808 nm, 3.25 W/cm^2, 1 min). (b) Average tumor weight of each group.

without laser exposure destroys tumor cells. Treatment efficiency of using laser illumination on tumors without plasmonic nanostructures is better than just only using GNRs@SiO_2 without laser illumination. However, coating DOX molecules onto the plasmonic composites (group 4) approximately reduces the tumor volume and weight by a factor of 1.5 and 2.7 compared to only GNR@SiO_2 (group 3) and saline injection (group 1), respectively. By turning on the NIR laser light when tumors have GNR@SiO_2-DOX, we combine the effects of the anticancer drug and photothermal agents. This combination significantly enhances the efficiency and effectiveness of GNR@SiO_2-DOX dose. Using more photothermal agents enables to absorb more optical energy to thermally devastate tumor tissue. One can deduce this conclusion from the comparison of groups 7 and 8, which correspond to injections with the optical densities of 5.5 and 9.2, respectively.

CONCLUSIONS

We have validated the anticancer effects of the chemo-photothermal therapy based on GNR@SiO_2-DOX by in vivo experiments. We have experimentally prepared GNR@SiO_2-DOX and examined complex structures via SEM and TEM imaging and XRD technique. Based on the absorption spectra, one can observe variations in plasmonic properties of GNRs of size 10.7 × 39.2 nm^2 when coating a mesoporous silica layer on the gold surface and encapsulating DOX molecules onto this silica layer. Moreover, these optical spectra allow us to determine the amount of loaded DOX molecules. After injecting solutions of GNR@SiO_2 and GNR@SiO_2-DOX into mice and scarifying them, photothermal experiments were carried out on both water and livers of the mice. These experiments prove that GNRs@SiO_2 are accumulated in livers. The mice liver can be approximately considered as a homogeneous medium and the injected GNRs are randomly dispersed in the liver when injected into mice. When we inject solutions of GNRs@SiO_2 and GNRs@SiO_2-DOX into tumor-implanted mice and irradiate NIR laser light on their tumors within 1 min after direct injection, health and weight of mice are observed every day for one month. Then, the weights of their tumors are measured. All measurements explicitly indicate that both chemotherapy and photothermal therapy significantly reduce tumor volumes. More reduction of volumes is found when these two approaches are combined.

ASSOCIATED CONTENT

Supporting Information

The Supporting Information is available free of charge at https://pubs.acs.org/doi/10.1021/acsomega.0c01939.

Average body weight of the nine groups of mice in in vivo experiments as a function of time, TEM image of the mesoporous silica coating on GNRs, and histogram of the rod length and width of GNRs (PDF)

AUTHOR INFORMATION

Corresponding Authors

Nghiem Thi Ha Lien − *Center for Quantum and Electronics, Institute of Physics, VAST, Hanoi 10000, Vietnam*; Email: halien@iop.vast.vn

Anh D. Phan − *Faculty of Materials Science and Engineering, Phenikaa Institute for Advanced Study and Faculty of Information Technology, Artificial Intelligence Laboratory, Phenikaa University, Hanoi 12116, Vietnam*; orcid.org/0000-0002-8667-1299; Email: anh.phanduc@phenikaa-uni.edu.vn

Authors

Bui Thi Van Khanh − *College of Science, Vietnam National University (VNU), Hanoi, Hanoi 10000, Vietnam*

Nguyen Thi Thuy − *Center for Quantum and Electronics, Institute of Physics, VAST, Hanoi 10000, Vietnam*

Nguyen Trong Nghia − *Center for Quantum and Electronics, Institute of Physics, VAST, Hanoi 10000, Vietnam*

Hoang Thi My Nhung − *College of Science, Vietnam National University (VNU), Hanoi, Hanoi 10000, Vietnam*

Tran Hong Nhung − *Center for Quantum and Electronics, Institute of Physics, VAST, Hanoi 10000, Vietnam*

Do Quang Hoa − *Center for Quantum and Electronics, Institute of Physics, VAST, Hanoi 10000, Vietnam*

Vu Duong − *Center for Quantum and Electronics, Institute of Physics, VAST, Hanoi 10000, Vietnam*

Nguyen Minh Hue − *Department of Physics, Le Quy Don Technical University, Hanoi 10000, Vietnam*

Complete contact information is available at: https://pubs.acs.org/10.1021/acsomega.0c01939

Notes

The authors declare no competing financial interest.

ACKNOWLEDGMENTS

The animal experiment and all in vivo studies were performed according to ethical approval (IRB-A-2001) and guidelines of the Institutional Review Board in Animal Research at Dinh Tien Hoang Institute of Medicine, Hanoi, Vietnam. The authors are grateful for the financial support for this work from the project VAST.CTVL.02/17-18 and the project 103.03-

2016.72 of the Vietnam National Foundation for Science and Technology Development (NAFOSTED).

REFERENCES

(1) Huang, X.; Jain, P. K.; El-Sayed, I. H.; El-Sayed, M. A. Plasmonic photothermal therapy (PPTT) using gold nanoparticles. *Lasers Med. Sci.* **2008**, *23*, 217−228.
(2) Abadeer, N. S.; Murphy, C. J. Recent Progress in Cancer Thermal Therapy Using Gold Nanoparticles. *J. Phys. Chem. C* **2016**, *120*, 4691−4716.
(3) Cole, J. R.; Mirin, N. A.; Knight, M. W.; Goodrich, G. P.; Halas, N. J. Photothermal Efficiencies of Nanoshells and Nanorods for Clinical Therapeutic Applications. *J. Phys. Chem. C* **2009**, *113*, 12090−12094.
(4) Link, S.; El-Sayed, M. A. Shape and size dependence of radiative, non-radiative and photothermal properties of gold nanocrystals. *Int. Rev. Phys. Chem.* **2000**, *19*, 409−453.
(5) Link, S.; Burda, C.; Mohamed, M. B.; Nikoobakht, B.; El-Sayed, M. A. Laser Photothermal Melting and Fragmentation of Gold Nanorods: Energy and Laser Pulse-Width Dependence. *J. Phys. Chem. A* **1999**, *103*, 1165−1170.
(6) O'Neal, D. P.; Hirsch, L. R.; Halas, N. J.; Payne, J. D.; West, J. L. Photo-thermal tumor ablation in mice using near infrared-absorbing nanoparticles. *Cancer Lett.* **2004**, *209*, 171−176.
(7) Wang, L.; Jiang, X.; Ji, Y.; Bai, Ru.; Zhao, Y.; Wu, X.; Chen, C. Surface chemistry of gold nanorods: origin of cell membrane damage and cytotoxicity. *Nanoscale* **2013**, *5*, 8384−8391.
(8) Yasun, E.; Li, C.; Barut, I.; Janvier, D.; Qiu, L.; Cui, C.; Tan, W. BSA modification to reduce CTAB induced nonspecificity and cytotoxicity of aptamer-conjugated gold nanorods. *Nanoscale* **2015**, *7*, 10240−10248.
(9) Shen, S.; Tang, H.; Zhang, X.; Ren, J.; Pang, Z.; Wang, D.; Gao, H.; Qian, Y.; Jiang, X.; Yang, W. Targeting Mesoporous Silica-Encapsulated Gold Nanorods for Chemo-Photothermal Therapy with Near-Infrared Radiation. *Biomaterials* **2013**, *34*, 3150−3158.
(10) Vallet-Regí, M.; Colilla, M.; Izquierdo-Barba, I.; Manzano, M. Mesoporous Silica Nanoparticles for Drug Delivery: Current Insights. *Molecules* **2018**, *23*, 47.
(11) Yang, H.; Xu, M.; Li, S.; Shen, X.; Li, T.; Yan, J.; Zhang, C.; Wu, C.; Zeng, H.; Liu, Y. Chitosan hybrid nanoparticles as a theranostic platform for targeted doxorubicin/VEGF shRNA co-delivery and dual-modality fluorescence imaging. *RSC Adv.* **2016**, *6*, 29685−29696.
(12) Chai, F.; Sun, L.; He, X.; Li, J.; Liu, Y.; Xiong, F.; Ge, L.; Webster, T. J.; Zheng, C. Doxorubicin-loaded poly (lactic-co-glycolic acid) nanoparticles coated with chitosan/alginate by layer by layer technology forantitumor applications. *Int. J. Nanomed.* **2017**, *12*, 1791.
(13) Li, G.; Chen, Y.; Zhang, L.; Zhang, M.; Li, S.; Li, L.; Wang, T.; Wang, C. Facile Approach to Synthesize Gold Nanorod@Polyacrylic Acid/Calcium Phosphate Yolk-Shell Nanoparticles for Dual-Mode Imaging and pH/NIR-Responsive Drug Delivery. *Nano-Micro Lett.* **2017**, *10*, No. 7.
(14) Zhang, Z.; Wang, J.; Nie, X.; Wen, T.; Ji, Y.; Wu, X.; Zhao, Y.; Chen, C. Near infrared laser-induced targeted cancer therapy using thermoresponsive polymer encapsulated gold nanorods. *J. Am. Chem. Soc.* **2014**, *136*, 7317−7326.
(15) Duong, V. T. T.; Phan, A. D.; Lien, N. T. H.; Hue, D. T.; Hoa, D. Q.; Nga, D. T.; Nhung, T. H.; Viet, N. A. Near-Infrared Photothermal Response of Plasmonic Gold-Coated Nanoparticles in Tissues. *Phys. Status Solidi A* **2018**, *215*, No. 1700564.
(16) Ayala-Orozco, C.; Urban, C.; Knight, M. W.; Urban, A. S.; Neumann, O.; Bishnoi, S. W.; Mukherjee, S.; Goodman, A. M.; Charron, H.; Mitchell, T.; Shea, M.; Roy, R.; Nanda, S.; Schiff, R.; Halas, N. J.; Joshi, A. Au Nanomatryoshkas as Efficient Near-Infrared Photothermal Transducers for Cancer Treatment: Benchmarking against Nanoshells. *ACS Nano* **2014**, *8*, 6372−6381.
(17) Wiley, D. T.; Webster, P.; Gale, A.; Davis, M. E. Transcytosis and brain uptake of transferrin-containing nanoparticles by tuning avidity to transferrin receptor. *Proc. Natl. Acad. Sci. U.S.A.* **2013**, *110*, 8662−8667.
(18) Blanco, E.; Shen, H.; Ferrari, M. Principles of nanoparticle design for overcoming biological barriers to drug delivery. *Nat. Biotechnol.* **2015**, *33*, 941−951.
(19) Kessentini, S.; Barchiesi, D. Quantitative Comparison of Optimized Nanorods, Nanoshells and Hollow Nanospheres for Photothermal Therapy. *Biomed. Opt. Express* **2012**, *3*, 590−604.
(20) Kim, M.; Lee, J.-H.; Nam, J.-M. Plasmonic Photothermal Nanoparticles for Biomedical Applications. *Adv. Sci.* **2019**, *6*, No. 1900471.
(21) Pigram, W. J.; Fuller, W.; Hamilton, L. D. Stereochemistry of Intercalation: Interaction of Daunomycin with DNA. *Nature New Biol.* **1972**, *235*, 17−19.
(22) Tacar, O.; Sriamornsak, P.; Dass, C. R. Doxorubicin: an update on anticancer molecular action, toxicity and novel drug delivery systems: Doxorubicin cell and molecular biological activity. *J. Pharm. Pharmacol.* **2013**, *65*, 157−170.
(23) Waterhouse, D. N.; Tardi, P. G.; Mayer, L. D.; Bally, M. B. A Comparison of Liposomal Formulations of Doxorubicin with Drug Administered in Free Form: Changing Toxicity Profiles. *Drug Saf.* **2001**, *24*, 903−920.
(24) Zhang, M.; Jiang, L. Doxorubicin Hydrochloride-Loaded Mesoporous Silica Nanoparticles Inhibit Non-Small Cell Lung Cancer Metastasis by Suppressing VEGF-Mediated Angiogenesis. *J. Biomed. Nanotechnol.* **2016**, *12*, 1975−1986.
(25) Liu, Y.; Xu, M.; Chen, Q.; Guan, G.; Hu, W.; Zhao, X.; Qiao, M.; Hu, H.; Liang, Y.; Zhu, H.; Chen, D. Gold nanorods/mesoporous silica-based nanocomposite as theranostic agents for targeting near-infrared imaging and photothermal therapy induced with laser. *Int. J. Nanomed.* **2015**, *10*, 4747−4761.
(26) Schwartz, J. A.; Shetty, A. M.; Price, R. E.; Stafford, R. J.; Wang, J. C.; Uthamanthil, R. K.; Pham, K.; McNichols, R. J.; Coleman, C. L.; Payne, J. D. Feasibility study of particle-assisted laser ablation of braintumors in orthotopic canine model. *Cancer Res.* **2009**, *69*, 1659−1667.
(27) Gad, S. C.; Sharp, K. L.; Montgomery, C.; Payne, J. D.; Goodrich, G. P. Evaluation of the Toxicity of Intravenous Delivery of Auroshell Particles (Gold-Silica Nanoshells). *Int. J. Toxicol.* **2012**, *31*, 584−594.
(28) Rastinehad, A. R.; Anastos, H.; Wajswol, E.; Winoker, J. S.; Sfakianos, J. P.; Doppalapudi, S. K.; et al. Gold nanoshell-localized photothermal ablation of prostate tumors in a clinical pilot device study. *Proc. Natl. Acad. Sci. U.S.A.* **2019**, *116*, 18590−18596.
(29) Ye, X.; Jin, L.; Caglayan, H.; Chen, J.; Xing, G.; Zheng, C.; Doan-Nguyen, V.; Kang, Y.; Engheta, N.; Kagan, C. R.; et al. Improved Size-Tunable Synthesis of Monodisperse Gold Nanorods through the Use of Aromatic Additives. *ACS Nano* **2012**, *6*, 2804−2817.
(30) Shen, J.; He, Q.; Gao, Y.; Shi, J.; Li, Y. Mesoporous silica nanoparticles loading doxorubicin reverse multidrug resistance: performance and mechanism. *Nanoscale* **2011**, *3*, 4314−4322.
(31) Yan, T.; Cheng, J.; Liu, Z.; Cheng, F.; Wei, X.; He, J. pH-Sensitive mesoporous silica nanoparticles for chemo-photodynamic combination therapy. *Colloids Surf., B* **2018**, *161*, 442−448.
(32) Li, C.; Feng, K.; Xie, N.; Zhao, W.; Ye, L.; Chen, B.; Tung, C.-H.; Wu, L.-Z. Mesoporous Silica-Coated Gold Nanorods with Designable Anchor Peptides for Chemo-Photothermal Cancer Therapy. *ACS Appl. Nano Mater.* **2020**, *3*, 5070−5078.
(33) Beijnen, J. H.; Wiese, G.; Underberg, W. J. Aspects of the chemical stability of doxorubicin and seven other anthracyclines in acidic solution. *Pharm. Weekbl., Sci.* **1985**, *7*, 109−116.
(34) Richardson, H. H.; Carlson, M. T.; Tandler, P. J.; Hernandez, P.; Govorov, A. O. Experimental and Theoretical Studies of Light-to-Heat Conversion and Collective Heating Effects in Metal Nanoparticle Solutions. *Nano Lett.* **2009**, *9*, 1139−1146.
(35) von Maltzahn, G.; Park, J. H.; Agrawal, A.; Bandaru, N. K.; Das, S. K.; Sailor, M. J.; Bhatia, S. N. Computationally Guided

https://dx.doi.org/10.1021/acsomega.0c01939
ACS Omega 2020, 5, 20231−20237

Photothermal Tumor Therapy Using Long-Circulating Gold Nanorod Antennas. *Cancer Res.* **2009**, *69*, 3892−3900.
(36) Sadauskas, E.; Wallin, H.; Stoltenberg, M.; Vogel, U.; Doering, P.; Larsen, A.; Danscher, G. Kupffer Cells Are Central in the Removal of Nanoparticles from the Organism. *Part. Fibre Toxicol.* **2007**, *4*, 10.

https://dx.doi.org/10.1021/acsomega.0c01939
ACS Omega 2020, 5, 20231−20237